Should the Master Equatorial Be a Slave?

W. Gawronski,[1] H. G. Ahlstrom, Jr.,[1] and A. M. Bernardo[1]

The article describes the existing 70-m antenna control system, the master equatorial (ME) control system, and their "master–slave" interaction through the autocollimator coupling. The analysis describes the open-loop models of the antenna and ME, obtained through field tests and system identification. Next, the performances of closed-loop systems of the antenna and ME are evaluated. The closed-loop performance indicates that a single control algorithm can replace three existing algorithms and that the mode-switching algorithm is no longer required. This new single control algorithm provides significant performance improvement at minimal cost, using primarily existing equipment.

Different configurations of the antenna and ME are proposed and evaluated. In the existing configuration, the ME is a master: it follows a target, and the antenna is a slave, following the ME. This arrangement causes occasional problems. Since antenna drives were designed for rates smaller than 0.25 deg/s and for accelerations smaller than 0.2 deg/s^2, tracking at high rates (e.g., near the keyhole) may leave the antenna outside the autocollimator acquisition range. It causes the breakdown of the ME–antenna optical link and termination of the track. Here we analyze two new ME–antenna configurations. Configuration A is a modification of the existing configuration with new control algorithms and a command preprocessor added, where the antenna follows the ME. Configuration B also includes new control algorithms and a command preprocessor, but unlike Configuration A, the ME is a slave and follows the antenna. It serves, in effect, as an antenna position sensor. Analysis shows that both configurations are feasible for high-rate tracking using the existing autocollimator. Configuration B, however, is superior as it has much smaller autocollimator errors. Finally, for the existing configuration and for Configurations A, there is no provision for ME wrap direction, while Configuration B would simplify identification of wrong ME wrap and make it easier to derive a recovery scheme.

There are two tracking modes: the autocollimator and encoder modes. Switching between the two is necessary when the autocollimator link is terminated. Switching is a concern because it creates jerks and antenna oscillations. Since the switching in the existing configuration causes excessive jerks, a special filter is implemented to suppress them. Analysis shows that switching jerks in Configurations A and B are

[1] Communications Ground Systems.

The research described in this publication was carried out by the Jet Propulsion Laboratory, California Institute of Technology, under a contract with the National Aeronautics and Space Administration.

small; thus, the switching does not need a dedicated algorithm for jerk reduction. A comparison of the characteristics of the existing configuration and Configurations A and B is given.

I. Introduction

The 70-m antenna control system consists of the antenna control itself and of the master equatorial (ME). The ME is a small telescope mounted on the top of a tower, close to the focal point of the antenna. An optical instrument (autocollimator) creates a link between the antenna dish and the ME. The ME is a master: it is commanded to follow a target. The antenna is a slave; using an optical coupling (autocollimator), it follows the ME. The antenna, as a slower device, may lag behind the ME and stay out of the range of the autocollimator or maintain significant slow oscillations in and out of the autocollimator beam range, causing the termination of control.[2] When out of range, the control system switches from the autocollimator to the encoders, and the tracking continues. The switching causes antenna jerking (different algorithms control the autocollimator and encoder modes) and loss of precision (the encoders are less precise than the autocollimator).

Tracking precision can be improved, and switching during tracking can be avoided. This article presents two new control configurations of improved tracking precision that additionally prevent switching during tracking and prevent oscillations and jerking when switching is necessary. Configuration A is a modification of the current ME–antenna configuration, and Configuration B is a reconfigured control system such that the ME is a slave and follows the antenna. It effectively serves as a position sensor. In the latter configuration, the ME, a light and fast device, virtually never lags significantly behind the antenna.[3] The purpose of this article is to analyze both configurations.

In order to carry on the analysis, first we give details on system identification of the antenna open-loop systems (with encoders and the autocollimator as position sensors) and on the system identification of the ME. Next, the results of the design of the antenna and the ME controllers are presented, followed by the description of the two configurations of the antenna and ME control systems, and ending with evaluation of the performances of these two configurations.

A significant part of this article is committed to improvement of performance through introduction of a single algorithm to control the antenna. Currently four control algorithms reside in the antenna servo controller:

(1) A slew mode, or the large-error-mode algorithm

(2) A computer[4] tracking mode, or the small-error-mode algorithm

(3) A precision tracking-mode algorithm

(4) A mode-switching algorithm

The analysis presented in this article shows that

---

[2] A common breakdown of this optical link occurs during lockup near the zenith keyhole during high-elevation acquisitions; it may include slow oscillations. Stowing the antenna from near-zenith also can cause a similar breakdown in which the elevation pre-limits are entered.

[3] The exception is the North Polar keyhole, where the required ME rates are high.

[4] The current terms "computer mode" and "precision mode" do not reflect the true natures of the modes. In the computer mode, encoder feedback is used; in the precision mode, autocollimator feedback is used. Thus, in the following, we replace the terms computer mode with "encoder mode" and precision mode with "autocollimator mode."

(1) A single control algorithm can drive the antenna.

(2) A single (autocollimator) mode is needed for tracking.

(3) Configurations A and B satisfy the requirement for tracking without switching. However, autocollimator error in the latter configuration is much smaller than in Configuration A.

(4) The encoder mode is not required for tracking and will serve as a backup mode, a service mode, or for initial positioning of the ME and the antenna, should a significant angular difference exist between the ME and the antenna.

(5) If switching between the encoder and autocollimator modes is required, a special algorithm and a dedicated filter are not needed.

II. Open-Loop Tests

The block diagram of the current control system configuration of a 70-m antenna is shown in Fig. 1. It consists of the antenna rate loop (antenna structure and the drives) and two controllers: the precision-mode controller (in the following, called the autocollimator-mode controller) and the computer-mode controller (in the following, called encoder-mode controller). It consists also of the ME rate loop (ME instrument and its drives), ME controller, and autocollimator. System identification tests were conducted, and the locations of the test signal injections and of the measurement points for the antenna and ME tests are shown in this figure.

The purpose of the open-loop tests is to determine the open-loop antenna azimuth-axis and elevation-axis models and the ME hour-axis and declination-axis models. The models are later used in the antenna and ME controller design. The antenna tests will supply information on structural resonances and on differences between the encoder loop (encoders used as sensors) and autocollimator loop (the autocollimator used as a sensor). The ME tests confirmed that the ME is a higher-bandwidth device.

A. Open-Loop Antenna Tests

1. Test Signal Description. White noise was used for testing purposes. The noise is "white" if its bandwidth (or sampling rate) is much larger than a test article bandwidth. The open-loop antenna bandwidth does not exceed 10 Hz; therefore, we select the noise bandwidth of 23 Hz. The length of the noise record is also selected, having in mind that the number of samples in the record will be expressed in powers of two. The test records are divided into sections and averaged; therefore, the longer the record, the better. But, the required memory and the span of the test time limit the record length. Our experience shows that a record of $16,382 = 2^{14}$ samples results in satisfactory accuracy of the signal processing, while a shorter record produces rather noisy results.

2. Procedure. White noise is injected into the closed-loop system at the location denoted "antenna test signal" in Fig. 1. The closed-loop system, rather than the open-loop system, is tested despite the fact that the tests will determine open-loop models. The feedback loop is closed in order to prevent antenna drift outside the autocollimator acquisition range and to make possible the autocollimator reading. The input voltage for the azimuth or elevation axis at measurement point MP1 in Fig. 1 is recorded, along with the azimuth or elevation encoder (measurement point MP2 in Fig. 1) and the autocollimator hour angle and declination angle readings (measurement point MP3 in Fig. 1). Note that at measurement point MP1 the recorded signal is a sum of the injected noise and the feedback signal.

3. Transfer Function and Coherence from the Data. Denote by u the input signal at point MP1 and by y the response of the encoder or the autocollimator. The first 1000 samples of u and y records are shown in Fig. 2; the sampling time was $\Delta t = 1/23 = 0.0435$ s. The open-loop transfer function is determined using the input and output data and the Matlab procedure spectrum.

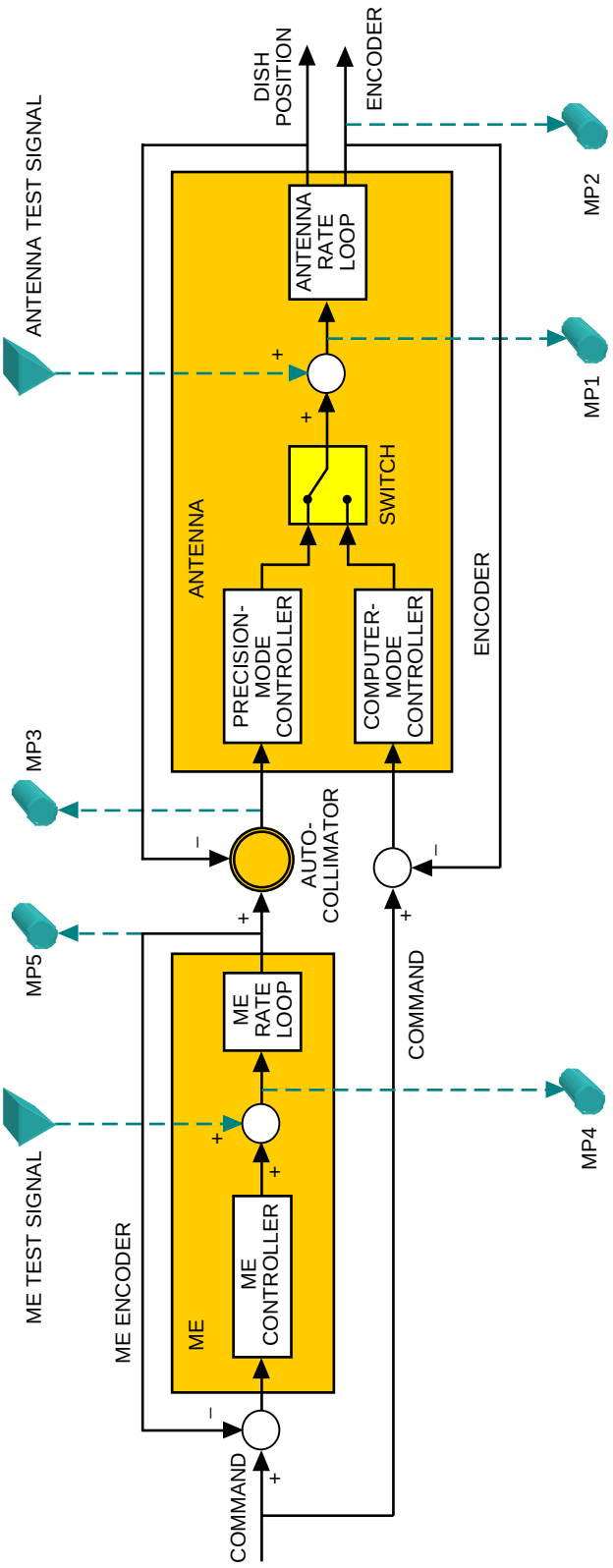

Fig. 1. The existing configuration of the antenna and ME (measurement points are denoted MP, and signal injection points are marked with triangles).

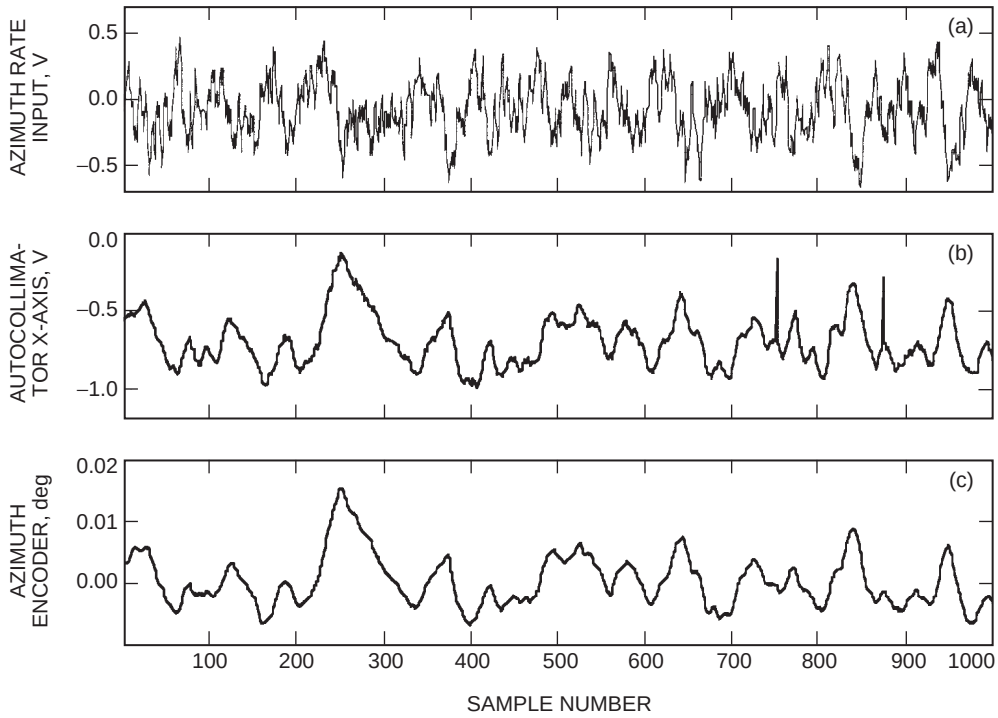

Fig. 2. The first 1000 of DSS-63 antenna test 1: (a) the input, the rate voltage, (b) the first output, the autocollimator x-axis reading, and (c) the second output, the azimuth encoder reading.

The sampling time, Δt (or sampling frequency, $f_o = 1/\Delta t$), defines the highest frequency, f_c, of the transfer function. This band-limiting frequency or Nyquist frequency is half of the sampling frequency

$$f_c = \frac{1}{2\Delta t} = \frac{f_o}{2} \tag{1}$$

In our case, $\Delta t = 0.0435$ ($f_o = 23$ Hz); thus, $f_c = 11.5$ Hz.

The frequency resolution of the spectra, Δf, is obtained from the length of the record, N, and from the sampling time, Δt, namely

$$\Delta f = \frac{1}{N\Delta t} = \frac{f_o}{N} \tag{2}$$

It is, at the same time, the lowest frequency of the spectra. In our case, the total length of the record was divided into 16 segments of 1024 samples, and $f_o = 23$ Hz; thus, $\Delta f = 0.0225$ Hz.

The quality of the data is evaluated through the coherence function between input u and output y. This function is non-negative and does not exceed 1. It is 1 when y is a linear function of u and there is no other variable that influences y. Thus, coherence is a measure of the linearity of the relationship between the input and output and a measure of the exclusiveness of the relationship between the input and output. For our purposes, coherence larger than 0.9 indicates reliable data; if it is less than 0.6, the quality of the data is poor. When it is between 0.6 and 0.9, the data can be accepted if the reason for the low coherence is known.

The estimate of the transfer function between the rate input and the autocollimator is plotted in Fig. 3 (dashed line). It shows a slope of 20 dB/dec and phase of −90 deg in the low frequency range. A resonance peak is visible at a frequency of 1.1 Hz and noise above 5 Hz. The estimate of the transfer function between the rate input and the azimuth encoder output was obtained and is plotted in Fig. 4. The quality of this transfer function is evaluated by the coherence function, shown in Fig. 5. It is of high value up to 1.3 Hz, weakly coherent at frequencies of 2 Hz and 2.4 Hz, and of low coherence at frequencies above 2.5 Hz.

4. Determination of the Open-Loop Model from the Field Data. The collected input and output data allow for the determination of an analytical model of a system, which in our case is the state–space representation (A, B, C) of the open-loop model. We used the SOCIT code of the NASA Langley Research Center (see [1]), and the method is described in [2].

The results of the system identification are presented in the following figures. In Figs. 3 and 4, the transfer functions of the identified azimuth-axis models are presented as solid lines. It can be noted that there is good coincidence between the identified and the measured transfer functions in the frequency regions where the coherence is high. Magnitudes of the transfer functions for the elevation open loop are shown in Figs. 6 and 7, where the solid lines are from the identified model and the dashed lines are directly from the input and output data. The test results also showed higher resonance peaks at the autocollimator than at the encoder location.

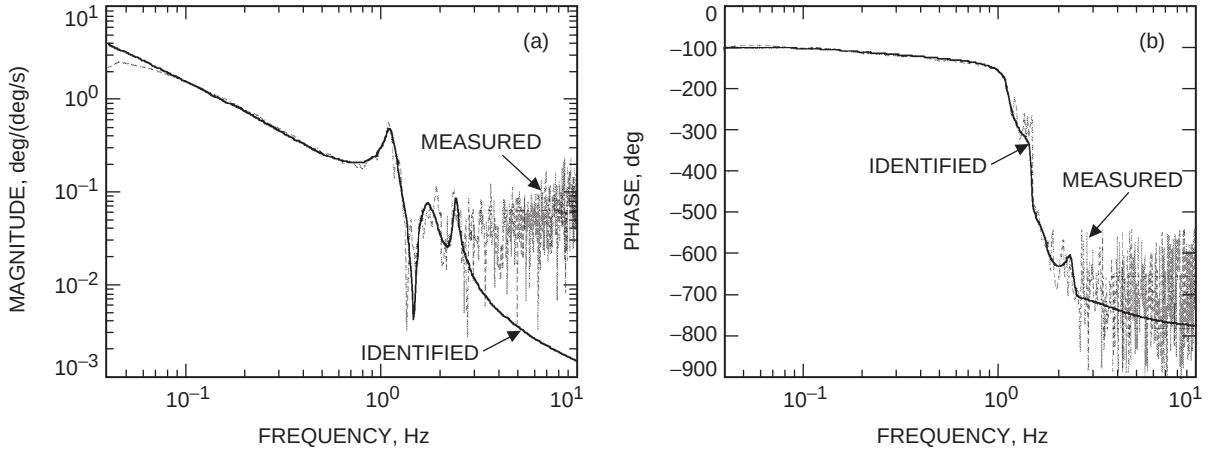

Fig. 3. DSS-63 azimuth-axis autocollimator-mode transfer function: (a) magnitude and (b) phase.

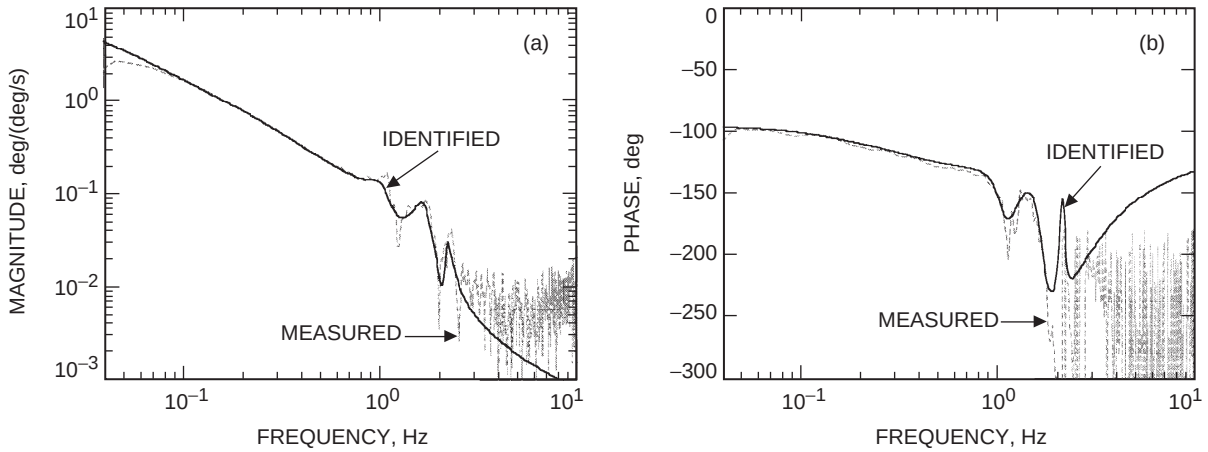

Fig. 4. DSS-63 azimuth encoder-mode transfer function: (a) magnitude and (b) phase.

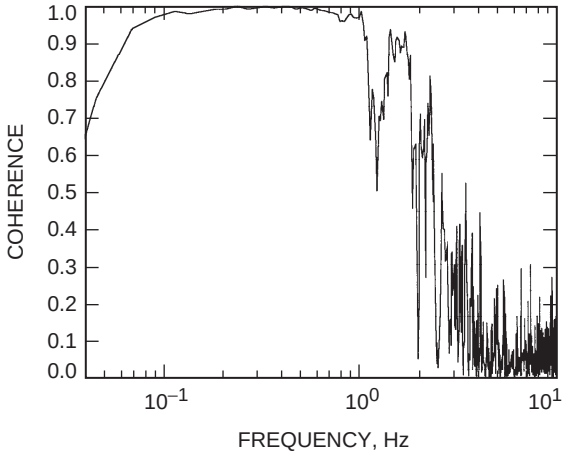

Fig. 5. Coherence of the DSS-63 azimuth encoder-mode transfer function.

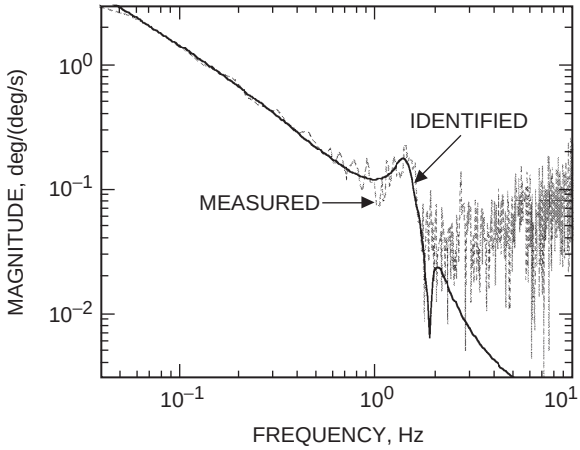

Fig. 6. Magnitude of the DSS-63 elevation-axis autocollimator-mode transfer function.

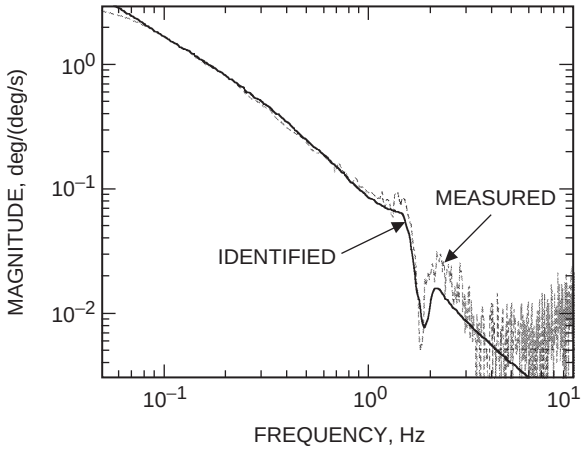

Fig. 7. Magnitude of the DSS-63 elevation encoder-mode transfer function.

5. Model Comparison. The multiple tests on two antennas allowed for comparison of the DSS-14 (at Goldstone) and DSS-63 (at Madrid) antenna models. Figures 8 and 9 show the system identification repeatability results for (a) three consecutive tests of the azimuth axis and (b) two tests of the elevation axis. Note that the results are quite repeatable up to a frequency of 4 Hz. Note also that in both azimuth- and elevation-axis data the resonance peaks are much higher at the autocollimator location than at the encoder locations. A possible explanation is that the alidade vibrations at this frequency are more intensive at the top than at the bottom. It also means that the encoders are not good devices to sense the flexible motion of the antenna at the focal point.

The identified models of the DSS-14 and DSS-63 antennas are compared in Figs. 10 and 11. The magnitudes of the transfer functions show the same pattern, although the resonant frequencies are slightly shifted, and the elevation-axis transfer functions of the DSS-14 antenna have higher resonant peaks than the transfer functions of the DSS-63 antenna. The azimuth-axis transfer functions of the DSS-14 antenna have lower resonant peaks than the transfer functions of the DSS-63 antenna. Part of the frequency differences could be fluctuations of the sampling time of about ± 2.5 percent during data collection.

Not exactly coincidental, the natural frequencies of the DSS-14 and DSS-63 models are compared in Tables 1 and 2.

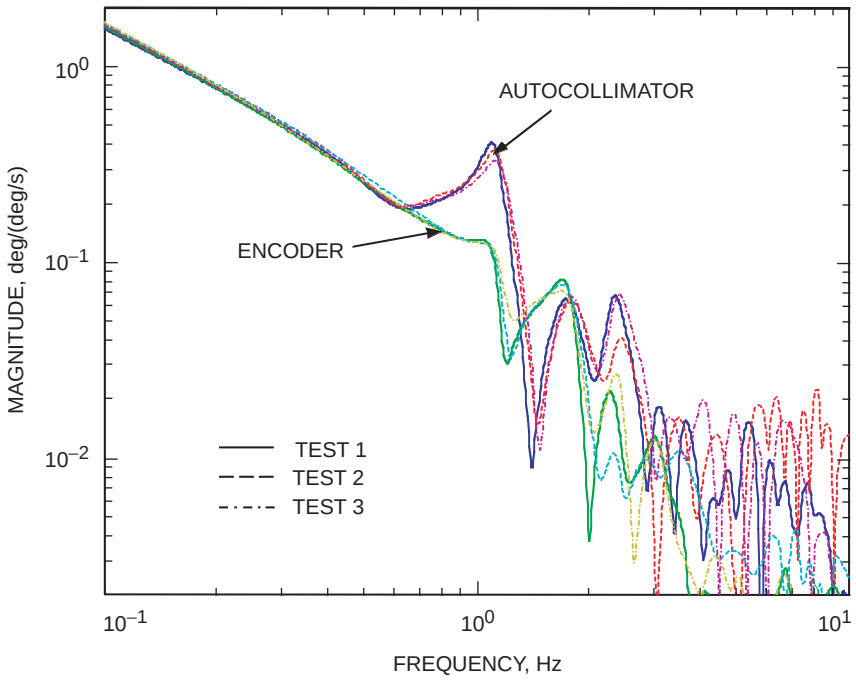

Fig. 8. Magnitudes of the DSS-63 azimuth-axis transfer function for the three consecutive tests.

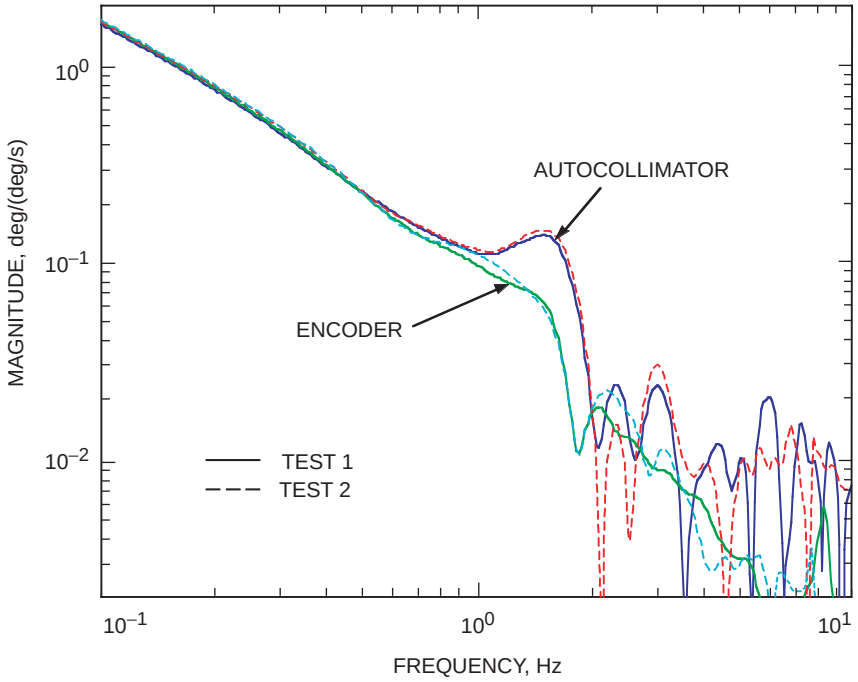

Fig. 9. Magnitudes of the DSS-63 elevation-axis transfer function for the two consecutive tests.

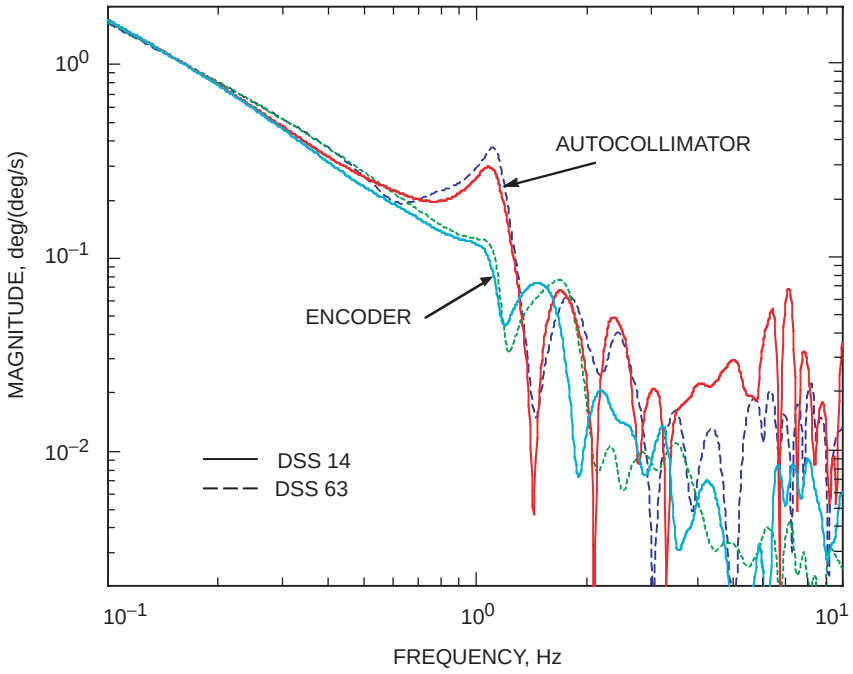

Fig. 10. Magnitudes of the DSS-14 and DSS-63 azimuth-axis transfer functions.

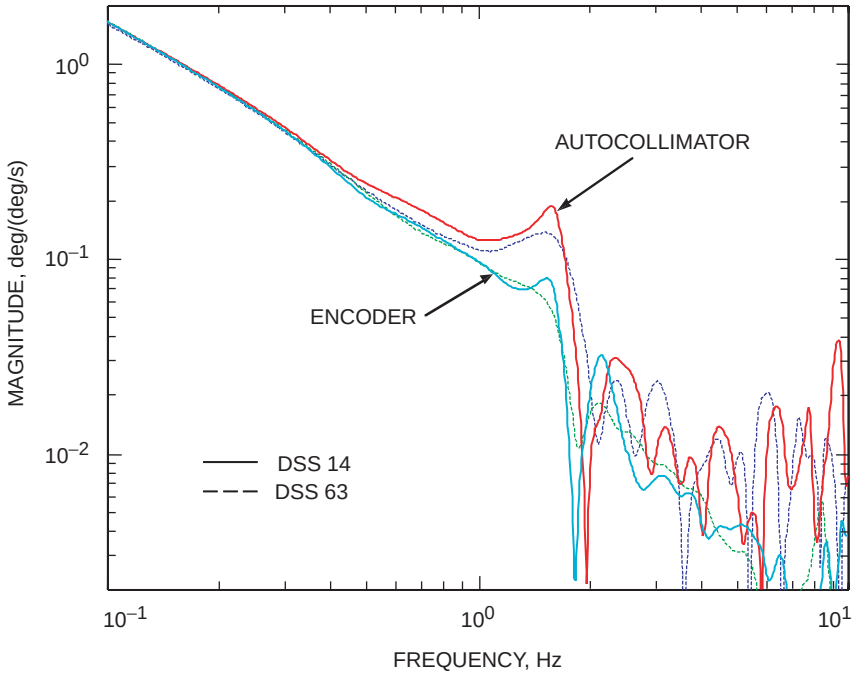

Fig. 11. Magnitudes of the DSS-14 and DSS-63 elevation-axis transfer functions.

Table 1. Azimuth-axis natural frequencies.

Antenna	First natural frequency, Hz	Second natural frequency, Hz	Third natural frequency, Hz	Fourth natural frequency, Hz
DSS 14	0.57	1.13	1.65	2.25
DSS 63	0.62	1.14	1.77	2.41

Table 2. Elevation-axis natural frequencies.

Antenna	First natural frequency, Hz	Second natural frequency, Hz	Third natural frequency, Hz	Fourth natural frequency, Hz
DSS 14	0.46	0.51	1.62	2.21
DSS 63	0.54	0.73	1.64	2.41

B. Open-Loop Master Equatorial Tests

The ME test points are marked MP4 and MP5 in Fig. 1. The input signal at point MP4 represents total input to the ME (consisting of the ME test signal and the feedback signal), and the ME encoder is recorded at point MP5. The ME is a rigid instrument; therefore, within a 10 Hz antenna bandwidth, it behaves as an integrator. Indeed, consider the transfer function of the ME hour axis of the DSS-63 antenna in Fig. 12. The slope of the transfer function magnitude is −20 dB/dec, and the phase is −90 deg. These are values representing an integrator, or a rigid body structure. The coherence of the data is high—above 0.97, as shown in Fig. 13. Similar results were obtained for the hour axis of the DSS-14 ME and the declination axes of the DSS-63 and DSS-14 MEs.

III. Closed-Loop Systems

The design of the closed-loop system of a 70-m antenna with encoders as position sensors was presented in [3]. Here, we extend the design to both encoder and autocollimator sensors. The ME closed-loop system performance is also presented in terms of step responses and of transfer functions.

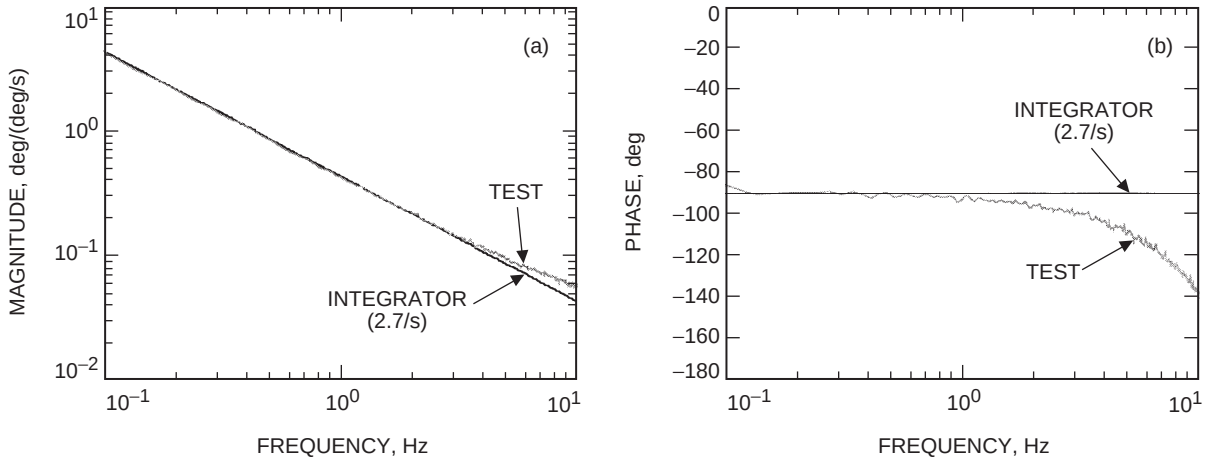

Fig. 12. The DSS-63 ME transfer functions, hour axis: (a) magnitude and (b) phase.

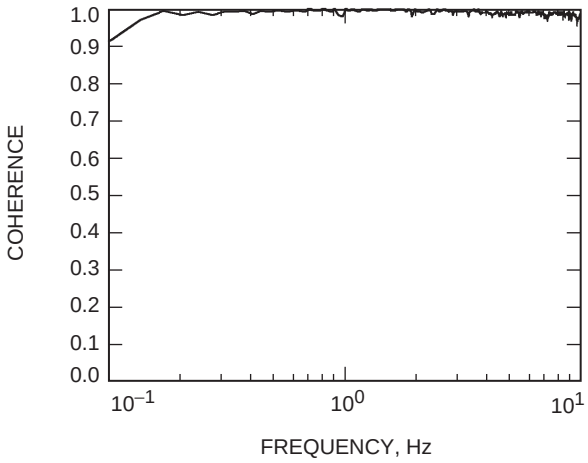

Fig. 13. Coherence of the DSS-63 ME transfer functions, hour axis.

A. Antenna Closed-Loop: A Single Algorithm for the Autocollimator and Encoder Modes

Currently four control algorithms reside in the antenna servo controller:

(1) A slew mode, or the large-error-mode algorithm

(2) A computer tracking mode, or the small-error-mode algorithm

(3) A precision tracking-mode algorithm

(4) A mode-switching algorithm

The slew mode is used to slew the antenna over large angular displacements. It is used for large-angle slewing when the rate and acceleration limits are reached, causing instability. The computer tracking mode is used to track predicts with the encoder feedback. It is used when the autocollimator is outside signal acquisition range, e.g., when commanding an antenna at rates that surpass the maximum allowable rate. In the precision mode, the antenna attempts to follow the master equatorial using autocollimator feedback. In addition to the three algorithms, a special algorithm switches from one mode to another [4].

The objective is to evaluate the performance of the encoder and autocollimator modes and to introduce a single control algorithm for all modes, so that mode switching is not necessary except on special occasions.

There are three reasons that four different algorithms have to be used:

(1) The rate and acceleration limits are hit when slewing using one of the non-slew algorithms.

(2) The autocollimator error exceeds ±110 mdeg, or 220 mdeg peak-to-peak.

(3) The switching algorithm is necessary because each mode is controlled by separate control algorithms.

Implementing a command preprocessor algorithm solves the first problem. A command preprocessor (CPP) is described in [5]. It prevents the antenna commands from exceeding the imposed rate and acceleration limits of 0.25 deg/s and 0.2 deg/s^2, respectively. With the introduction of the command preprocessor, there is no need for a separate control algorithm for slewing. The second problem is resolved by implementation of the CPP and the linear-quadratic-Gaussian (LQG) controller, so that the

autocollimator error is less than 220 mdeg. Implementing identical control algorithms for the encoder and autocollimator modes solves the third problem. Switching in this case causes a minimal jerk. This approach is described later.

The control-system structure is shown in Fig. 14. It consists of the antenna open-loop system (the antenna structure and the drives) obtained from the system identification tests and of a controller. The antenna controller is shown in Fig. 15. It is an LQG controller, described in [3]. Separate LQG controllers were designed for each axis. Their performances in terms of step responses, transfer function bandwidths, and rms servo error due to wind gusts is given below.

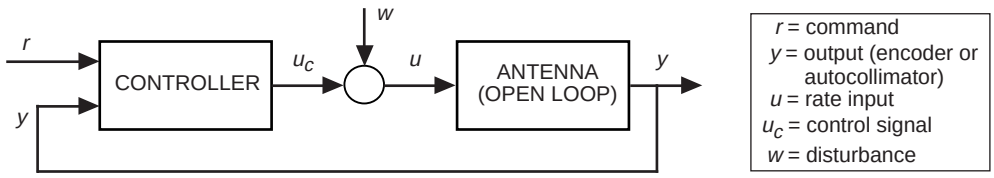

Fig. 14. The closed-loop system.

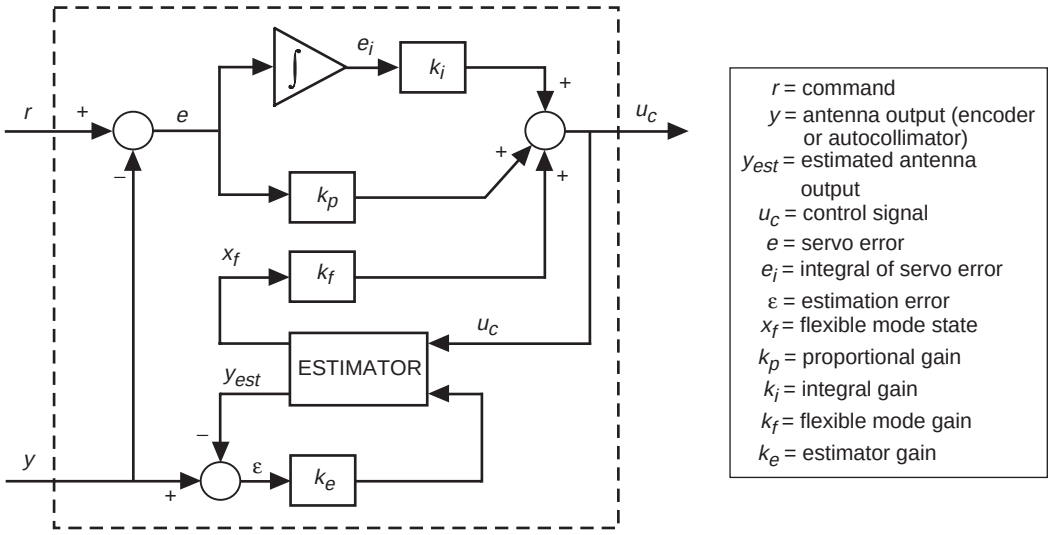

Fig. 15. The antenna LQG controller.

1. Azimuth-Axis Controller Performance. The responses to the 10-mdeg step of the azimuth encoder and the azimuth autocollimator are shown in Fig. 16. The settling time in both cases is 2 s; overshoot is 44 percent at the autocollimator and 32 percent at the encoder. The autocollimator also has a small undershoot.

The magnitudes of the closed-loop transfer functions are shown in Fig. 17 for the autocollimator and for the encoder outputs. The closed-loop bandwidth is 1.3 Hz for the autocollimator and 0.6 Hz for the encoder. The rms error in 32 km/h wind is 0.43 mdeg at the autocollimator and 0.40 mdeg at the encoder.

2. Elevation-Axis Controller Performance. The responses to the 10-mdeg step of the elevation encoder and the elevation autocollimator are shown in Fig. 18. The settling time in both cases is 2.2 s; overshoot is 35 percent at the autocollimator and 22 percent at the encoder.

The magnitudes of the closed-loop transfer functions are shown in Fig. 19 for the autocollimator and the encoder outputs. The closed-loop bandwidth is 1.8 Hz for the autocollimator and 0.8 Hz for the encoder. The rms error in 32 km/h wind is 1.30 mdeg at the autocollimator and 1.21 mdeg at the encoder.

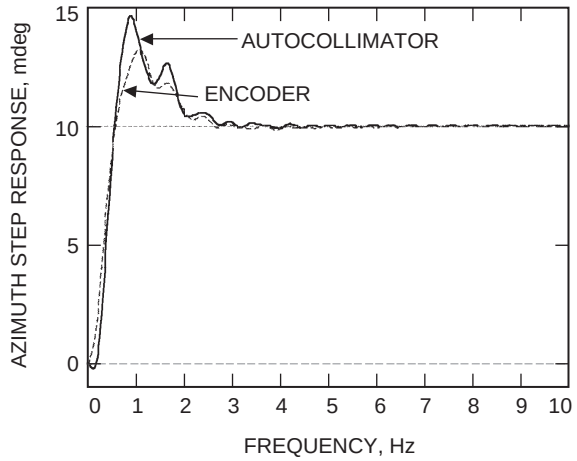

Fig. 16. Closed-loop responses of the autocollimator and the encoder to azimuth 10 mdeg step offset.

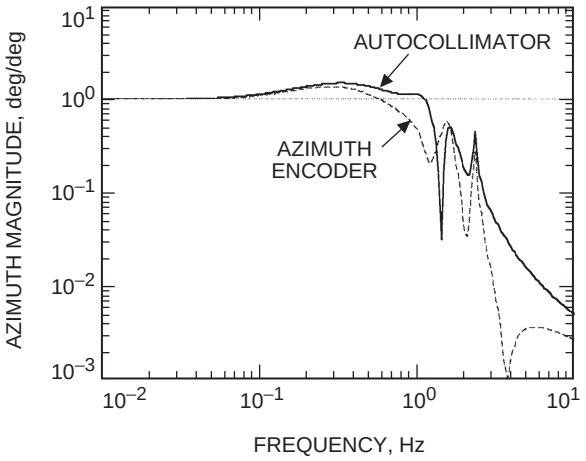

Fig. 17. Magnitudes of the closed-loop transfer function: autocollimator and encoder, azimuth axis.

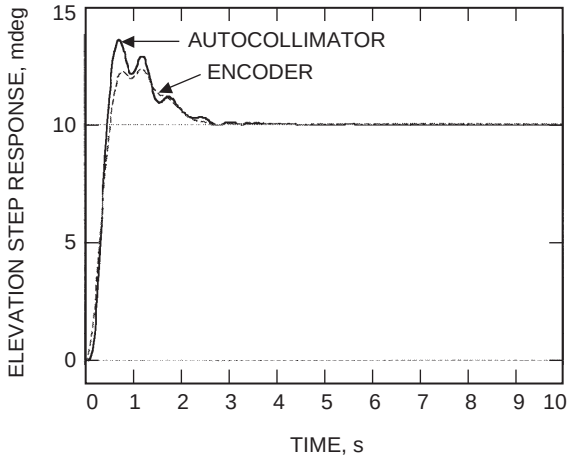

Fig. 18. Closed-loop responses of the autocollimator and the encoder to elevation 10 mdeg step offset.

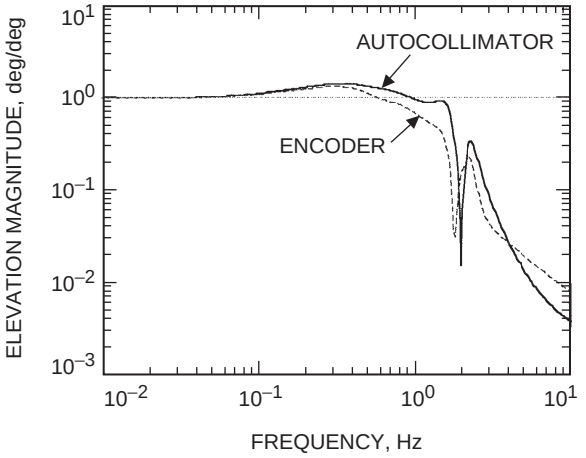

Fig. 19. Magnitudes of the closed-loop transfer function, autocollimator, and encoder, elevation axis.

B. ME Closed-Loop Performance

The ME control system has the same arrangement as the antenna system shown in Fig. 14, except that the antenna open-loop system is replaced with the ME open-loop system (obtained from the system identification) and the antenna controller is replaced with the ME controller. The ME controller is shown in Fig. 20. It is a proportional-and-integral controller with a feedforward loop. Its proportional gain is $k_p = 20$, and the integral gain is $k_i = 10$. The ME step response (see Fig. 21) has a small (2 percent) overshoot and a small (0.2 s) settling time. The ME bandwidth is 3.5 Hz; see the plot of magnitude of the transfer function in Fig. 22. The performance of the ME exceeds the antenna performance, as required. Namely, the ME settling time is much smaller than the antenna settling time, and the ME bandwidth is much wider than the antenna bandwidth.

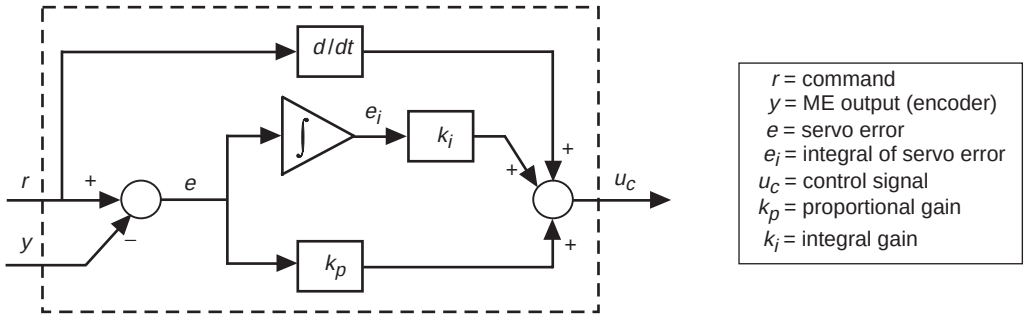

Fig. 20. The ME controller.

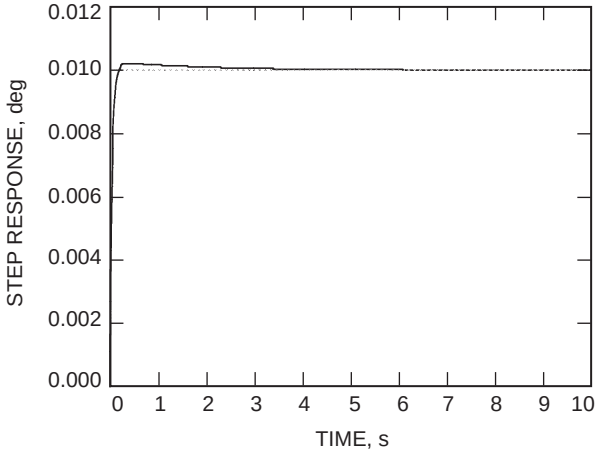

Fig. 21. The ME step response.

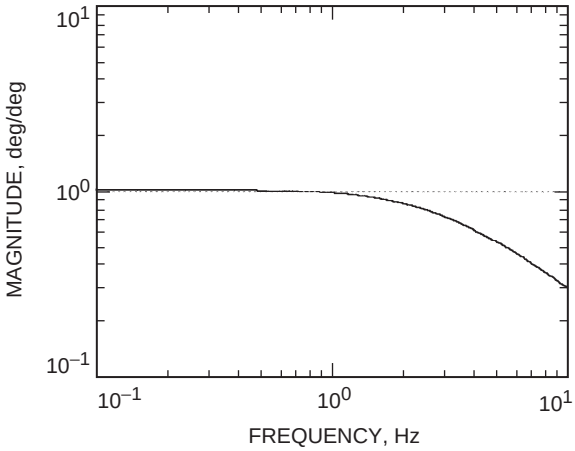

Fig. 22. Magnitude of the ME transfer function.

IV. New Configurations of the ME and Antenna

The combined performance of the ME and antenna is analyzed in this section. The existing configuration of antenna and ME is shown in Fig. 1. The following new configurations are introduced and analyzed:

Configuration A: A modified existing control system, with an added command preprocessor and new control algorithms for the antenna and ME, and a single control algorithm for both the autocollimator and encoder modes.

Configuration B: A reconfigured control system, with the ME as a slave; it follows the antenna.

In Configuration A, the ME is commanded to follow a spacecraft, while the antenna, coupled with the ME through the autocollimator, follows the ME. The block diagram of this configuration is shown in Fig. 23. The main disadvantage of this configuration is the ability to decouple the ME and the antenna if the autocollimator acquisition is lost (i.e., when the error exceeds ±110 mdeg). It can happen because the ME, as a small and rigid device, can move much faster (up to 2 deg/s) than the heavy and flexible antenna (up to 0.25 deg/s). Therefore, in certain situations (such as tracking near the keyhole), the autocollimator signal is outside the acquisition range, causing the autocollimator mode to be switched into the encoder mode. The switching itself, as well as encoder usage, reduces the tracking precision.

In Configuration B, the ME follows the antenna rather than the antenna following the ME. Since the ME is much faster than the antenna, it will virtually never be left behind, and the autocollimator coupling will not be disconnected. In this configuration (shown in Fig. 24), the ME serves as the antenna position sensor (replacing the antenna encoders).

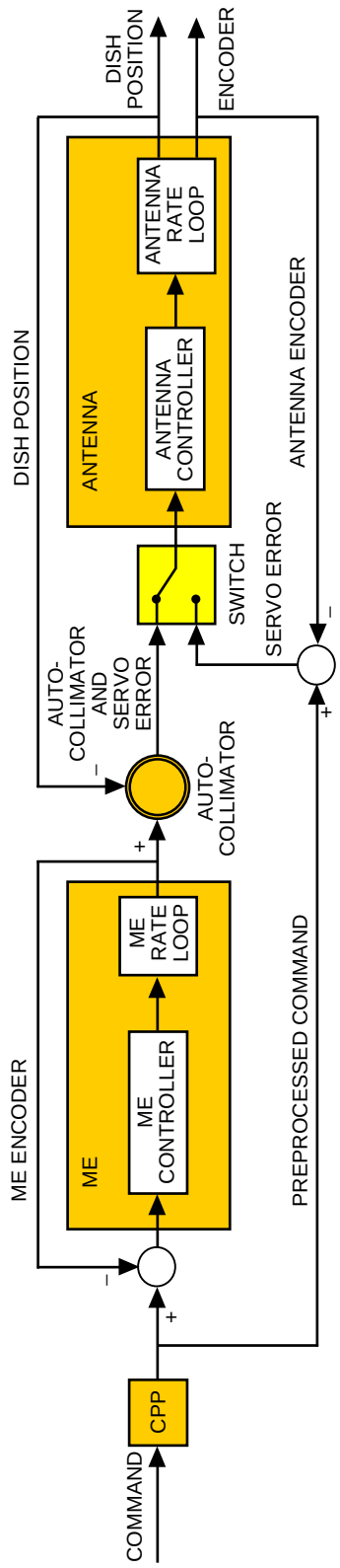

Fig. 23. Configuration A of the antenna and ME.

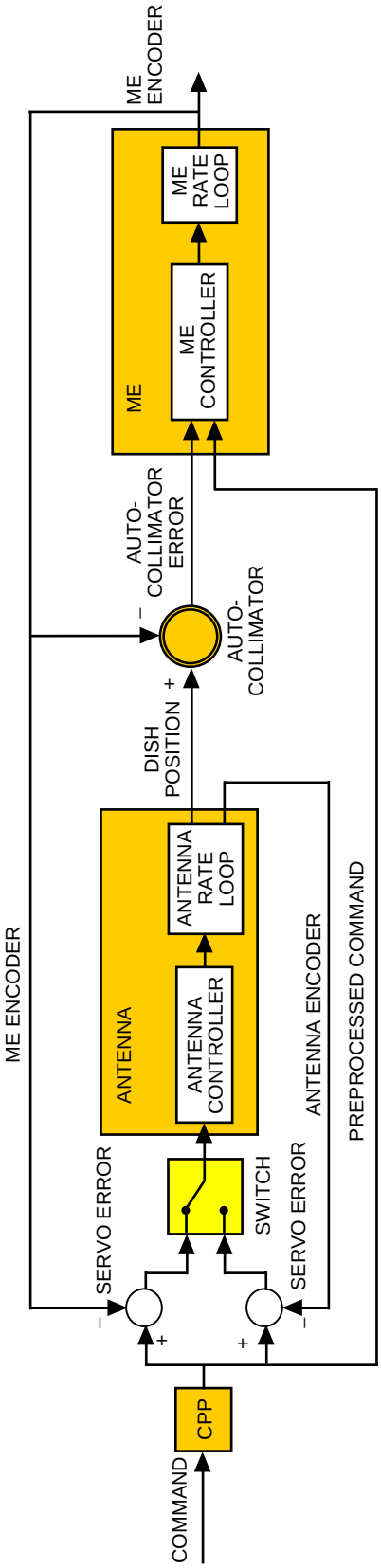

Fig. 24. Configuration B of the antenna and ME.

In the following subsection, the performances of Configurations A and B are simulated, and servo errors during switching are evaluated.

A. System Performance: Configurations A and B

The two configurations of the combined closed-loop systems, shown in Figs. 23 and 24, are tested using small (0.01 deg) and large (4 deg) steps and small (0.01 deg/s) and large (0.18 deg/s) rate offsets. Small commands are tested to ensure that the system behaves similarly to the antenna closed-loop system without the ME. Large-step commands verify if the magnitude of the autocollimator errors is smaller than the allowed 110 mdeg, since step commands cause the largest dynamic loads. The servo error and the autocollimator error were simulated. Note that in Configuration A the servo and autocollimator errors coincide, while in Configuration B they are measured at different locations, as shown in Figs. 23 and 24.

Since for Configuration A the servo and autocollimator errors are identical, they overlap in Figs. 25(a) through 25(d). These errors were obtained for small and large steps and for rate offsets. For Configuration B, the servo errors for small and large steps and rate offsets are shown in Figs. 26(a) through 26(d). The corresponding autocollimator errors are shown in Figs. 27(a) through 27(d). It follows from those figures that the servo errors for Configurations A and B are virtually the same. However, the autocollimator errors for Configuration B are much smaller than for Configuration A. It can be explained by the fact that the autocollimator error is the difference between the antenna position and the ME position. In Configuration B, the ME follows the antenna (see Fig. 24), and ME low inertia allows for fast following, resulting in small autocollimator errors. In Configuration A, the antenna follows the ME (see Fig. 23), and antenna large inertia results in slow following and large autocollimator errors.

In this subsection, we showed that the ME could not run away from the antenna in either Configuration A or Configuration B. However, in Configuration A the maximum autocollimator error was 110 mdeg, indicating that a drop in the antenna control system performance or excessive disturbance may

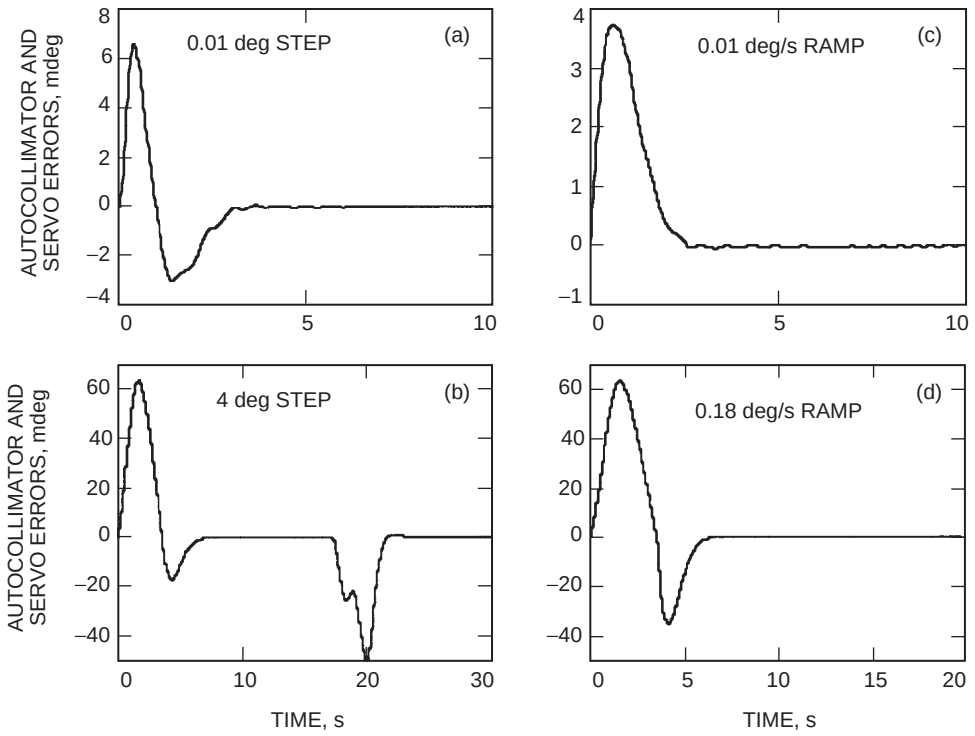

Fig. 25. Step and rate-offset autocollimator and servo errors of Configuration A: (a) small step, (b) large step, (c) small rate offset, and (d) large rate offset.

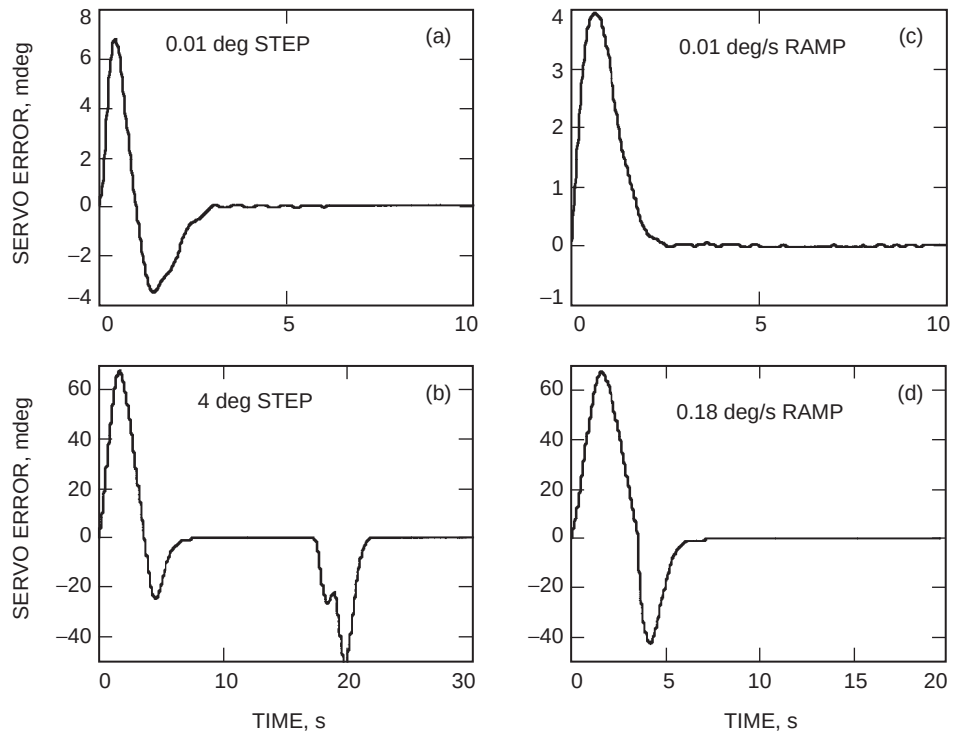

Fig. 26. Step and rate-offset servo errors of Configuration B: (a) small step, (b) large step, (c) small rate offset, and (d) large rate offset.

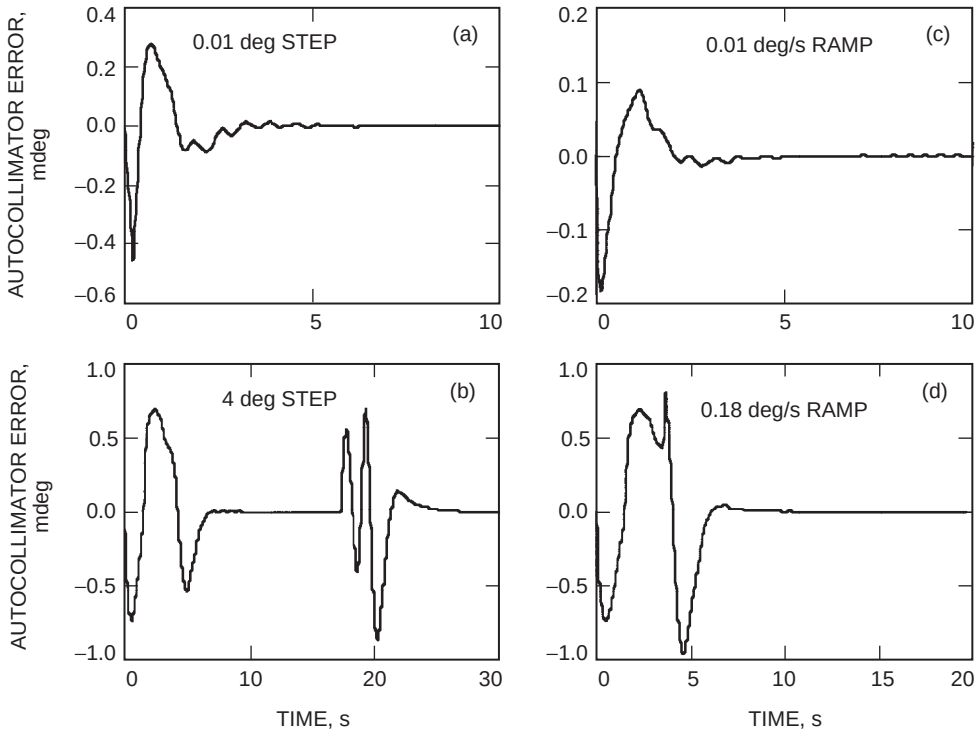

Fig. 27. Step and rate-offset autocollimator errors of Configuration B: (a) small step, (b) large step, (c) small rate offset, and (d) large rate offset.

occasionally result in autocollimator disconnection. In Configuration B, the antenna virtually cannot separate from the ME, since the maximum autocollimator error was very small, 2 mdeg.

B. Mode Switching

Despite satisfactory performance of Configuration A, switching between the autocollimator and encoder modes (or vice versa) may be necessary (e.g., in case of autocollimator failure). For this reason, we simulated switching between the two modes. The simulation diagram is shown in Fig. 28. The switching is triggered by a pulse function, see Fig. 29(a); its zero value switches to the encoder mode, and its unit value switches to the autocollimator mode. The antenna was commanded with a constant rate of 10 mdeg/s. The servo error (which is the autocollimator error in the autocollimator mode or the difference between the command and the encoder in the encoder mode) was simulated. It is small, as shown in Fig. 29(b); however, some transient dynamics were excited.

Next we simulated an unstable situation reported by Nickerson in [4]: a switching from the encoder to the autocollimator mode and vice versa with 30 mdeg misalignment between the autocollimator and the encoder.[5] We modeled this situation as a constant of 30 mdeg added to the encoder position, as in Fig. 28. With this misalignment and switching as shown in Fig. 30(a), the encoder readings in Figs. 30(b) and 30(c) show a stable system in which the misalignment was canceled in 3 s.

V. Conclusions

This article described and analyzed two configurations of the antenna and ME. The goal was to have a single control algorithm and a single mode to track and to slew. The goal was achieved by taking the following steps.

First, the test results allowed for development of accurate antenna and ME models using system identification procedures. In this article, models of the antenna and ME were derived and described. The obtained models showed that structural amplitudes at the autocollimator and the encoders are not identical, that the models of DSS 14 and DSS 63 are similar, and that the tests, despite their random nature, are repeatable. It also was shown that ME models in the hour axis and the declination axis are rigid body models, i.e., there are no flexible deformations of the ME within the antenna bandwidth.

Next, the antenna and ME controllers were designed. The antenna controller is of the LQG type, while the ME controller is a proportional-and integral controller with a feedforward loop. The new algorithms significantly improved antenna tracking precision.

Third, two new configurations of the antenna and ME combined system were studied: Configuration A (where a slave antenna follows a master ME) and Configuration B (where a slave ME follows a master antenna). The analysis shows that both configurations work satisfactorily using a single control algorithm. Namely, Configuration A, with the addition of the command preprocessor and new control algorithm, can be used in slewing, tracking, and scanning since the maximal autocollimator error is 110 mdeg (peak-to-peak), and thus is smaller than the maximum allowable error of 220 mdeg. For Configuration B, the analysis shows that autocollimator errors are very small (less than 2 mdeg peak-to-peak), showing that this configuration is better fitted for slewing, tracking, and scanning.

Fourth, switching between the encoder and autocollimator modes was simulated. The analysis showed that switching jerks are small (both in Configurations A and B) and that the system is stable. A comparison of the characteristics of Configurations E, A, and B of the 70-m antenna control system is given in Table 3.

[5] At high elevations (near the zenith keyhole), a 500 mdeg discrepancy may separate the encoder and autocollimators in azimuth angles. In cross-elevation, this separation can be between 50 and 90 mdeg, even at low elevations.

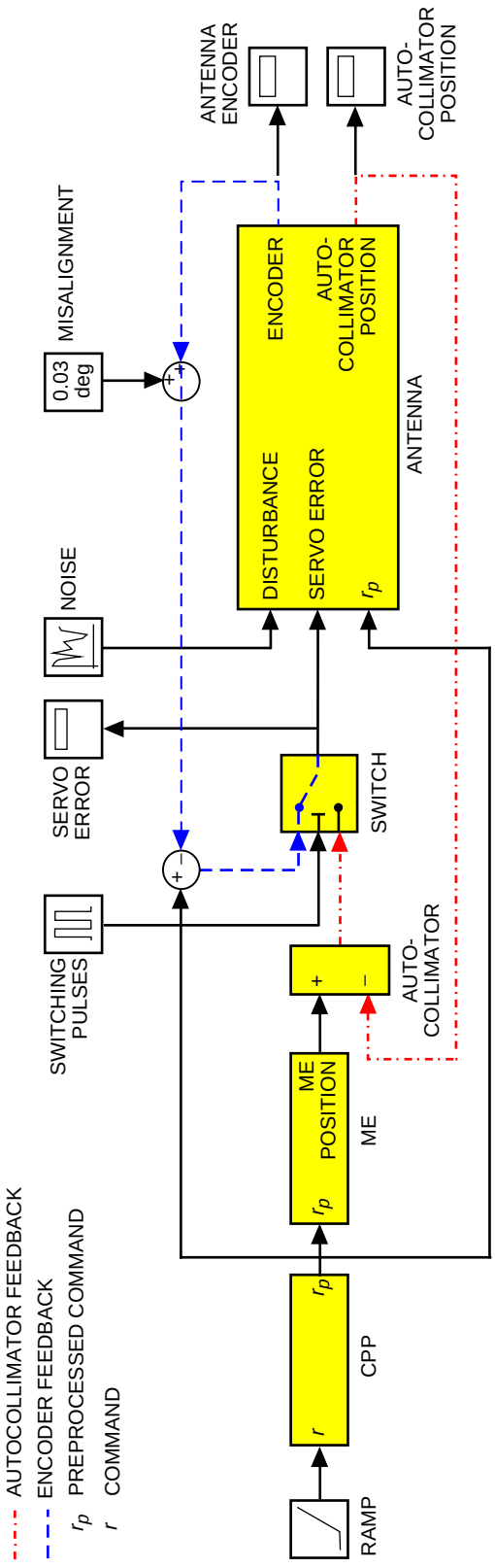

Fig. 28. Simulink model of the autocollimator/encoder mode switching.

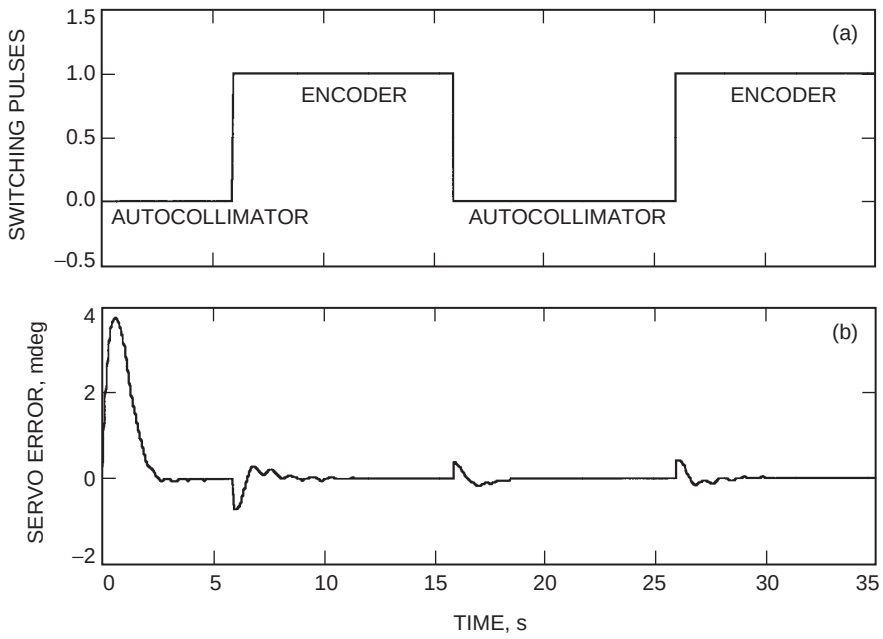

Fig. 29. Mode switching: (a) switching pulses and (b) servo error during switching.

Table 3. Features of the 70-m antenna control system configurations.

Feature	Existing configuration	Configuration A	Configuration B
Number of control algorithms	3	1	1
Number of tracking modes	2, with switching	1, occasional switching	1
Is a mode-switching algorithm required?	Yes	No	No

Acknowledgments

The authors would like to thank David Girdner for technical discussions and assisting in the antenna testing and measurements and Robert Haroldsson for assisting in the antenna testing and measurements.

References

[1] J. N. Juang, L. G. Horta, and M. Phan "System/Observer/Controller Identification Toolbox," NASA Technical Memorandum 107566, 1992.

[2] J. N. Juang, *Applied System Identification*, Englewood Cliffs, New Jersey: Prentice Hall, 1994.

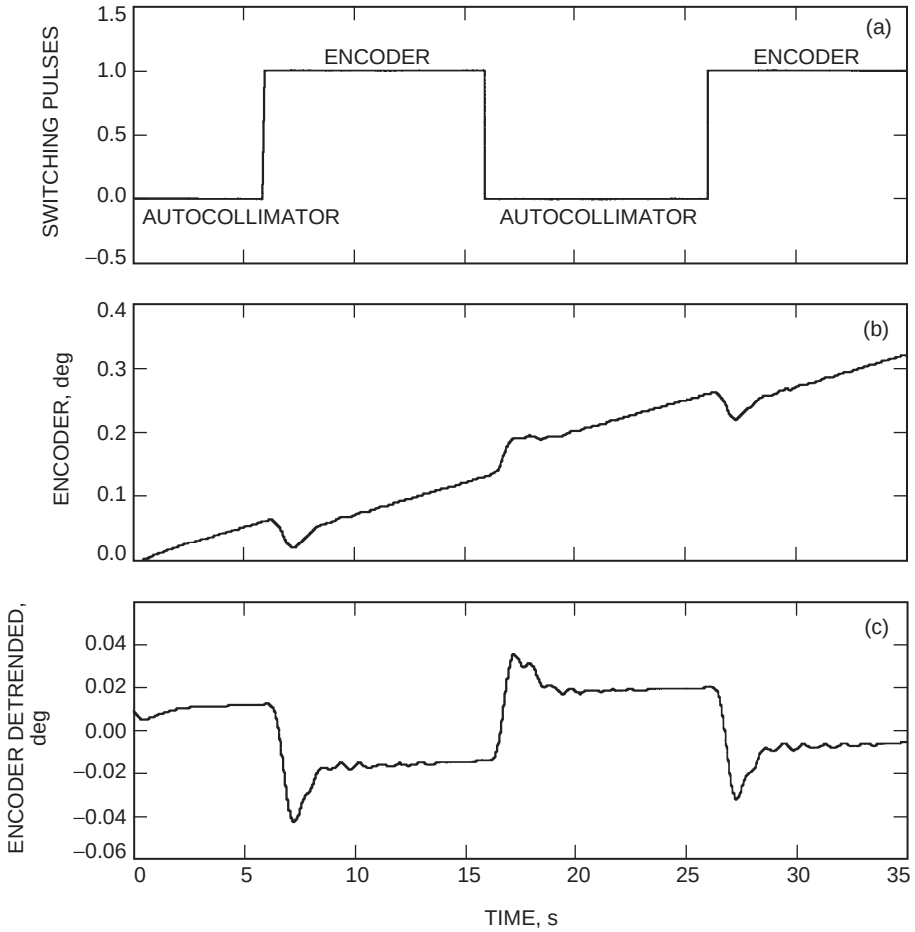

Fig. 30. The 30 mdeg misalignment between the autocollimator and encoder: (a) switching pulses, (b) antenna position during switching, and (c) detrended antenna position.

[3] W. Gawronski, H. G. Ahlstrom, Jr., and A. B. Bernardo, "Design and Performance of the DSS-14 Antenna Controller," *The Telecommunications and Mission Operations Progress Report 42-135, July–September 1998*, Jet Propulsion Laboratory, Pasadena, California, pp. 1–9, November 15, 1998.
http://tmo.jpl.nasa.gov/tmo/progress_report/42-135/135E.pdf

[4] J. A. Nickerson, "New Mode Switching Algorithm for the JPL 70-Meter Antenna Servo Controller," *The Telecommunications and Data Acquisition Progress Report 42-92, October–December 1987*, Jet Propulsion Laboratory, Pasadena, California, pp. 147–153, February 15, 1988.
http://tmo.jpl.nasa.gov/tmo/progress_report/42-92/92Q.PDF

[5] W. Gawronski, "Command Preprocessor for the Beam-Waveguide Antennas," *The Telecommunications and Mission Operations Progress Report 42-136, October–December 1998*, Jet Propulsion Laboratory, Pasadena, California, pp. 1–10, February 15, 1999.
http://tmo.jpl.nasa.gov/tmo/progress_report/42-136/136A.pdf